

Topological Spin Texture in a Quantum Anomalous Hall Insulator

Jiansheng Wu,¹ Jie Liu,¹ and Xiong-Jun Liu ^{*1,2}

¹*Department of Physics, Hong Kong University of Science and Technology, Clear Water Bay, Hong Kong, China*

²*Institute for Advanced Study, Hong Kong University of Science and Technology, Clear Water Bay, Hong Kong, China*
(Dated: December 2, 2024)

The quantum anomalous Hall (QAH) insulator, also called Chern insulator, is a two-dimensional (2D) topological state of quantum matter which exhibits a gap in the bulk and chiral gapless edge states in the boundary [1]. Different from the quantum Hall effect driven by external magnetic fields [2, 3], the QAH effect applies no magnetic field, and in the recent experimental discovery the spin-orbit coupling and ferromagnetic ordering are essential to reach this state [4]. In this work, we find a novel phenomenon in the Chern insulator that the edge states are chiral in both the orbital and spin degrees of freedom when a chiral-like symmetry is present, and exhibit topologically stable spin texture in the position space. The chiral edge spin texture has no correspondence in the conventional trivial materials, and may have potential applications in designing topological-state-based spin devices which might be applicable to future spintronic technologies.

Discovery of the quantum Hall effect in 1980s brought about a fundamental concept, topological state of quantum matter, to condensed matter physics [2, 3]. In the quantum Hall effect an external magnetic field drives the electrons to fill in discrete Landau levels. This leads to a gap in the 2D bulk, while the boundary exhibits 1D chiral gapless edge states, namely, the edge modes propagate one-way in each edge. In the integer quantum Hall effect the Hall conductance is quantized by Chern numbers, which are integers and characterize the global properties (topology) of the system [5]. The topological interpretation of the quantized Hall conductance implies that to obtain a quantum Hall state does not necessitate a magnetic field. The theoretical idea for quantum Hall effect without Landau levels, i.e. the QAH effect, was first introduced by Haldane in a honeycomb lattice over two decades ago [1]. The recent interests in this topological state have been revived due to the great development in the field of time-reversal invariant topological insulators [6, 7], with numerous new theoretical proposals having been introduced [8–13]. Importantly, following the proposal in Ref. [11], the QAH state has been detected in a recent experiment using ferromagnetic thin-film topological insulator, with the quantized Hall conductance having been observed [4].

The minimal model for the Chern insulator is described

by a two-band Hamiltonian $H = \sum_{\mathbf{k}} \psi_{\mathbf{k}}^{\dagger} \mathcal{H}(\mathbf{k}) \psi_{\mathbf{k}}$, where the spin basis $\psi_{\mathbf{k}} = (c_{\mathbf{k}\uparrow}, c_{\mathbf{k}\downarrow})^T$. Around the Γ point $\mathcal{H}(\mathbf{k})$ takes the simple (2 + 1)D Dirac form

$$\mathcal{H}(\mathbf{k}) = \begin{bmatrix} m_z + 2B(k_x^2 + k_y^2) & 2A_1k_y + i2A_2k_x \\ 2A_1k_y - i2A_2k_x & -m_z - 2B(k_x^2 + k_y^2) \end{bmatrix}, \quad (1)$$

where for the realization with thin-film ferromagnetic topological insulators [4, 11] m_z depends on the Zeeman term induced by the ferromagnetic order, the B -term characterizes the hybridization between top and bottom thin-film surfaces, and $2A_{1,2}$ equal Fermi velocities of the surface Dirac cones of the parent topological insulator [14, 15]. The QAH phase is obtained when $m_z B < 0$, with the Chern number $C_1 = \text{sgn}(m_z A_1 A_2)$ [11, 16]. In the solid-state experiment, the Cr-doped $(\text{Bi}_{1-x}\text{Sb}_x)_2\text{Te}_3$ was used to achieve the above Hamiltonian and the QAH phase [4]. On the other hand, this model can also be realized in a square optical lattice [17] with spin-orbit coupling generated based on cold atom experiments [18–20].

In the isotropic case $|A_1| = |A_2|$ the Hamiltonian (1) respects a chiral-like symmetry defined by $S = \sigma_{\vec{n}_1} \mathcal{M}_{\vec{n}_2}$, with $\vec{n}_1 \perp \vec{n}_2$ being arbitrary 2D orthogonal unit vectors in the x - y plane. Here $\sigma_{\vec{n}_1}$ and $\mathcal{M}_{\vec{n}_2}$ represent the \vec{n}_1 -component of the Pauli matrix acting on the spin space and the spatial reflection along the \vec{n}_2 direction, respectively. It can be seen that $S\mathcal{H}(\mathbf{k})S^{\dagger} = -\mathcal{H}(\mathbf{k})$. Then for two edges normal to \vec{n}_1 axis, the edge states with $k_{\vec{n}_2} = 0$ must be eigenstates of $\sigma_{\vec{n}_1}$, with the spin oppositely polarized in the opposite edges [21]. Furthermore, using the $\mathbf{k} \cdot \mathbf{p}$ theory one can expand the 1D edge Hamiltonian up to the leading order of momentum and confirm that the edge states with nonzero $k_{\vec{n}_2}$ are also eigenstates of $\sigma_{\vec{n}_1}$. This result is shown numerically in Fig. 1. We see that the spin of edge states is in-plane polarized, and varies one cycle following the 1D closed path of the boundary. This spin texture shows that the edge states are chiral in both the orbital and spin degrees of freedom. Interestingly, the spin chirality gives a nontrivial quantized Berry phase for the edge modes after evolving one cycle along the boundary: $\gamma_C = \pm\pi$, and this defines a 1D winding number $\mathcal{N}_{1d} = \pm 1$ which can be verified to correspond to the bulk Chern invariant via $C_1 = \mathcal{N}_{1d} \text{sgn}(m_z)$. With fixed $\text{sgn}(m_z)$, changing the edge spin chirality reverses Chern number of the QAH insulator, while varying both the spin chirality and $\text{sgn}(m_z)$ gives the phases with the same C_1 (see e.g. Fig. 1 **a** and **f**). In Fig. 1 we have shown the chiral spin texture and edge currents of the 2D insulator in different parameter regimes, and with square (**a-d**) and circular (**e-h**) geometries, respectively.

*email: phylliuxiongjun@gmail.com

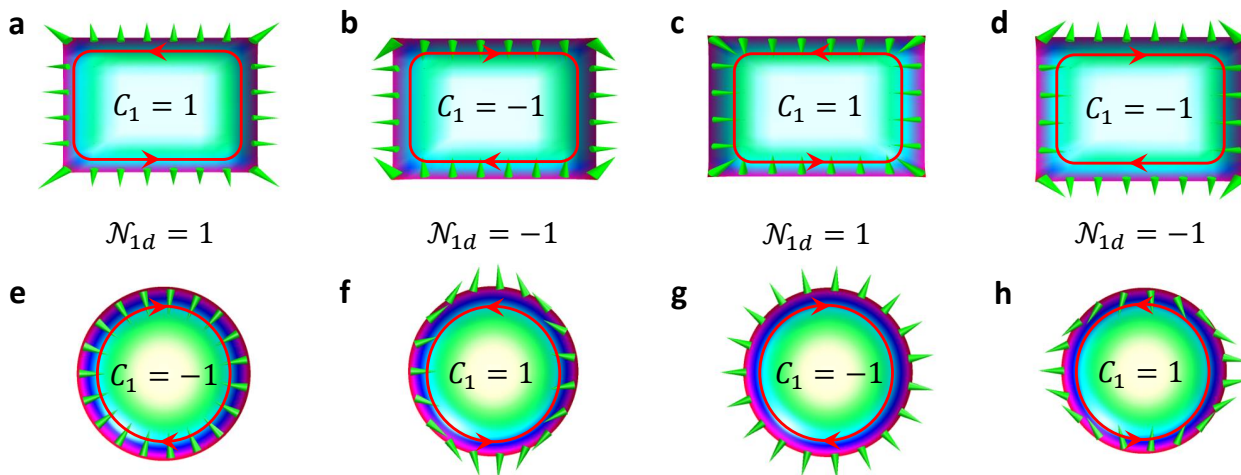


FIG. 1: **Topological spin texture of the edge states.** **a-d**, The edge spin texture for square geometry of the boundary, with the Zeeman term $m_z > 0$ and $B < 0$. **e-h**, The edge spin texture for circular geometry of the boundary, with $m_z < 0$ and $B > 0$. For the other parameters, we take that $A_1, A_2 > 0$ (**a,e**); $A_1 > 0, A_2 < 0$ (**b,f**); $A_1, A_2 < 0$ (**c,g**); and $A_1 < 0, A_2 > 0$ (**d,h**). The topological spin textures give rise to quantized Berry phases if evolving the edge spin one circle along the boundary, which define 1D nontrivial topological states in the position space of the boundary and characterized by the 1D winding number \mathcal{N}_{1d} . The bulk Chern number C_1 corresponds to \mathcal{N}_{1d} with an additional sign factor $\text{sgn}(m_z)$.

The above study demonstrates a correspondence between the nontrivial topologies exhibited in the bulk and the boundary. The bulk Chern number is a topological invariant of the first Brillouin zone, which is a 2D closed manifold in the momentum space due to the band gap of the insulator. However, the edge modes are gapless and generically the 1D boundary is a closed manifold not in the momentum space, but in the position space. Therefore the 1D edge invariant \mathcal{N}_{1d} is obtained in the real space rather than in the \mathbf{k} -space. Both the bulk and edge topological states are classified by integers Z . Note that a 1D topological state necessitates the symmetry protection [22]. The correspondence between the bulk and edge topological phases relies on the chiral-like symmetry as introduced above, albeit the Chern insulator is an intrinsic topological state not depending on symmetry. These properties implies that from an intrinsic bulk topological phase we obtain a real-space topological state in the reduced dimension of the boundary when the additional S symmetry is present.

While the 1D topological state relies on the symmetry protection, the chirality enables the topological spin texture to be insensitive to local perturbations which explicitly break the S symmetry. We have verified that the topological spin texture is stable against in-plane Zeeman fields without driving bulk phase transition, and insensitive to any type of local magnetic and nonmagnetic disorder scatterings, even when the disorder strength is comparable with the bulk gap. Actually, like that the orbital chirality of the edge modes prohibits the back scattering, the spin chirality ensures that no scattering occurs between two edge modes with opposite local spin polarizations. On the other hand, in the Methods section we show that the chiral spin texture may be scattered by

the discrete lattice anisotropy in the high-energy regime.

The edge channel of the Chern insulator can be described by 1D chiral Luttinger liquid [23, 24]. Furthermore, the above study shows that the edge modes are chiral in both orbital and spin degrees of freedom. As the topological spin texture leads to quantized Berry phases, which can be integrated by a Berry's connection, the edge states are governed by the following effective Hamiltonian

$$H_{\text{edge}} = iv_{\text{edge}} \int d\tilde{x} \psi_s^*(\tilde{x}) [\partial_{\tilde{x}} - i\mathcal{A}_s(\tilde{x})] \psi_s(\tilde{x}). \quad (2)$$

Here ψ_s denotes the orbital part of the edge states, \tilde{x} is the position parameter along the edge, and the Berry's connection $\mathcal{A}_s = i\hbar \langle \chi_s(\tilde{x}) | \partial_x | \chi_s(\tilde{x}) \rangle$, with $|\chi_s(\tilde{x})\rangle$ representing the polarized spin degree of freedom. The integral of \mathcal{A}_s along the 1D boundary gives $\oint d\tilde{x} \mathcal{A}_s(\tilde{x}) = \mathcal{N}_{1d}\pi$. The π -Berry phase is equivalent to a half magnetic flux-quantum threading through the 2D sample and encircled by the edge. According to the study by Wilczek in 1982 [25], a half quantum flux can lead to 1/2-fractionalization of the orbital angular momentum. As a result, for the 2D sample with circular geometry, the orbital angular momentum of the edge modes should be fractionalized as $l_z = m + \mathcal{N}_{1d}/2$, with m being integers. The fractionalization of the orbital angular momentum has an observable in the edge spectrum $\mathcal{E}_{l_z} = v_{\text{edge}} l_z R_{l_z}^{-1}$, with R_{l_z} the effective radius of edge state wave function. Due to the 1/2-fractionalization no zero-energy (mid-gap) edge state exists, and therefore the total number of edge states is *even*. However, threading an additional magnetic 1/2-flux-quantum can exactly push one original state to zero energy, changing the total number of edge modes to be *odd*, which provides an observable for the 1/2-fractionalization of orbital angular momentum.

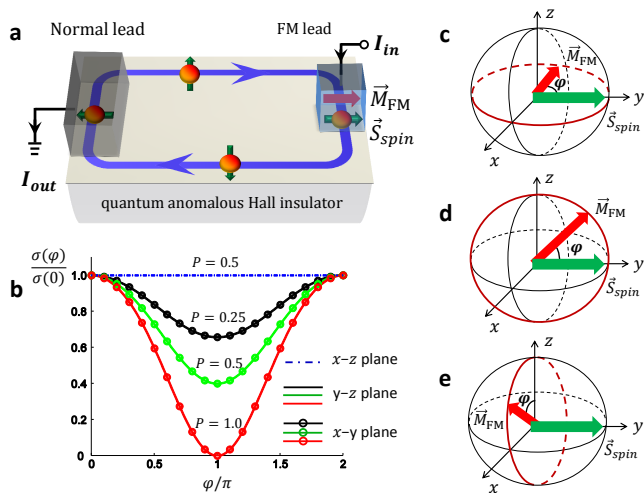


FIG. 2: **Angle-dependence of tunneling conductance.** **a**, A normal metallic lead is strongly coupled to the left-hand edge and a ferromagnetic lead is weakly coupled to the right-hand edge of the Chern insulator. Here the parameters for the quantum anomalous Hall phase satisfy $m_z > 0$, $A_{1,2} > 0$, and $B < 0$. Then spin of the edge states in the right-hand edge points to the $+y$ direction. **b**, The tunneling conductance $\sigma(\phi)$ is plotted versus azimuthal angle ϕ of the magnetization in the ferromagnetic lead, with the magnetization varying in the $x-y$ plane (**c**), $y-z$ plane (**d**), and $x-z$ plane (**e**), respectively. The numerical results are presented for different polarization ratios P in the ferromagnetic lead. The maximum tunneling conductance is obtained when the magnetization aligns with the edge spin-polarization direction.

The spin and orbital chirality make the edge of the Chern insulator be an exotic 1D metal which has no correspondence in conventional 1D materials. The topological spin texture of the edge modes may lead to strong spin-dependent effects as presented below, which on one hand can provide new unambiguous verification of the QAH state in the experiment, on the other hand, are applicable to spintronics by designing topological spin devices [26]. As illustrated in Fig. 2 **a**, we attach two metallic leads to the QAH sample, with a normal lead strongly coupled to the left-hand edge and a ferromagnetic lead weakly coupled to the right-hand edge. Due to the spin texture, the couplings between the sample edge and leads are fully spin selective, which can lead to strong anisotropic effects in the tunneling conductance when changing the direction of magnetization \vec{M}_{FM} in the ferromagnetic lead, as shown in Fig. 2 **b-e**. The tunneling conductance $\sigma(\phi)$ (Fig. 2 **b**) exhibits a clear angle-dependence when \vec{M}_{FM} varies in $x-y$ and $y-z$ planes (**c** and **d**), while it is a constant when \vec{M}_{FM} varies along $x-z$ plane (**e**). This measures that the edge spin polarizes to the y direction. The angle-dependence implies a strong magnetoresistive effect by setting \vec{M}_{FM} along $\pm y$ directions. The magnetoresistance, given by $\text{MR} = [\sigma(0) - \sigma(\pi)]/\sigma(\pi) \times 100\%$, is plotted in Fig. 3 as a function of chemical potential μ in the Chern in-

ulator and the polarization ratio P of the ferromagnetic lead. Due to the full spin-polarization, the edge of the sample can be regarded as an ideal dissipationless half-metal. This gives that $\text{MR} \approx 2P/(1-P) \times 100\%$, which is significantly larger than the corresponding tunneling magnetoresistance obtained in conventional ferromagnet/insulator/ferromagnet devices with the same polarization ratio (the inserted panel of Fig. 3) [27]. The strong magnetoresistive effect has been widely applied to spintronics, especially to designing read heads [26].

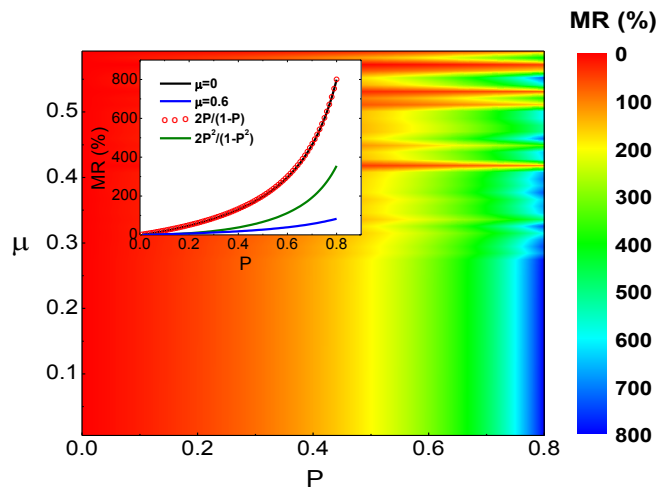


FIG. 3: **Magnetoresistance for the setup in Fig. 2a by setting magnetization of the ferromagnetic lead along $\pm y$ directions.** The magnetoresistance (MR) is plotted numerically as a function of the polarization ratio P in the ferromagnetic lead and the chemical potential μ (in unit of B) in the QAH insulator. The parameters for the QAH phase are taken as $m_z = -0.3A_{1,2} = -0.3B$, which gives the bulk gap $E_g = 2|m_z| = 0.6B$. The MR is uniform versus μ when the chemical potential is within the bulk gap ($|\mu| < 0.3B$) and decreases when μ lies out of the gap. The inserted panel shows that the MR coincides with $2P/(1-P)$ for $|\mu| < 0.3B$ (black solid and red circled curves), which is significantly larger than the corresponding tunneling MR, given by $2P^2/(1-P^2)$ (green curve), in the conventional ferromagnet/insulator/ferromagnet devices with polarization ratio P in both ferromagnets [27].

Another interesting application of the topological spin texture is to design controllable spin-filtering devices, as illustrated in Fig. 4. The edge spin texture ensures that the output current is fully spin-polarized, with the polarization direction depending on which edge the drain lead is attached to. From the numerical results we see that when the voltage of the output lead lies in the sample bulk gap, the output current is 100% polarized to the same direction, reflecting that the spin texture is identical for all edge states. We note that the band gap of the currently realized QAH effect is small, while for realistic applications a larger topological gap is necessary. The new physics unveiled in this work and the proposed potential applications will motivate the search for new novel

materials of Chern insulator with sizable band gaps in the future.

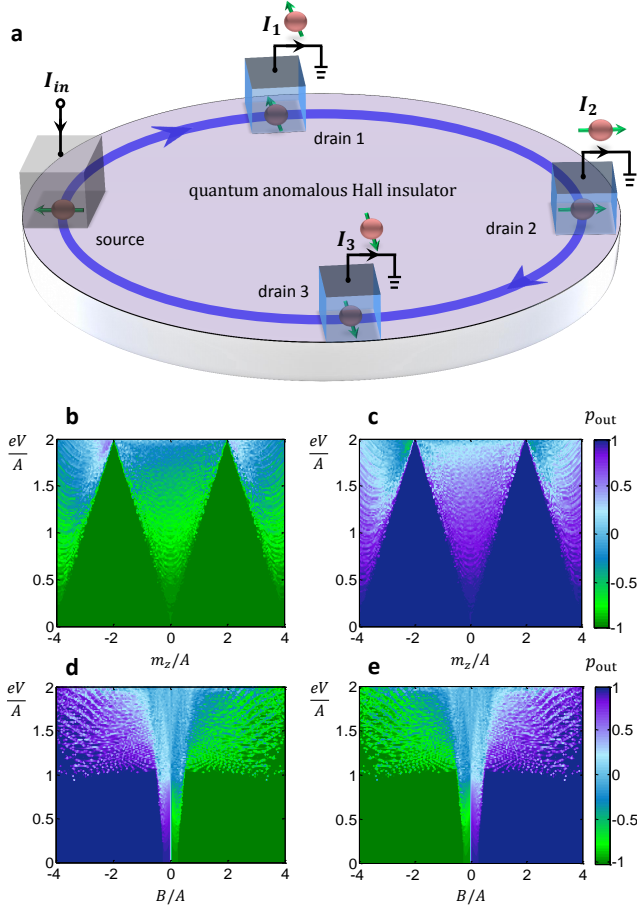


FIG. 4: Spin filtering effect and output spin-polarized current. **a**, For a quantum anomalous Hall insulator with circular boundary, the edge spin-polarization depends on the direction of the 1D edge. This provides a controllable way to generate spin-polarized current by attaching normal-metal leads to different directions of the sample edge. **b-e**, The polarization ratio p_{out} of the output spin current is plotted as a function of voltage eV in a drain lead and the Zeeman term m_z (**b,c**) or B (**d,e**), with the magnitudes rescaled by the spin-orbit coefficient A ($= |A_{1,2}|$). Other parameters are taken as $B = A_1 = A_2$ (**a**); $B = -A_1 = -A_2$ (**b**); $m_z = A_1 = A_2$ (**c**); and $m_z = -A_1 = -A_2$ (**d**). The sign change of p_{out} in **d** and **e** from the topological region with $B < 0$ to the region $B > 0$ implies that the edge spin reverses direction.

Methods

Lattice model. We consider the lattice model for the present QAH insulator, and require that the lattice Hamiltonian reduces to Eq. (1) around Γ point. The main results of this work are not lattice configuration dependent. Here we examine the following square lattice

Hamiltonian

$$\mathcal{H}(\mathbf{k}) = [m_z + 2Ba^{-2}(2 - \cos k_x a - \cos k_y a)]\sigma_z + 2A_1 a^{-1} \sin k_y a \sigma_x - 2A_2 a^{-1} \sin k_x a \sigma_y, \quad (3)$$

where a is the lattice constant and can be set as $a = 1$, and m_z is assumed to be $|m_z| < 4|B|$ for convenience. The above Hamiltonian describes a topological (trivial) phase for $m_z B < 0$ ($m_z B > 0$), with the Chern number $C_1 = \text{sgn}(A_1 A_2)[\text{sgn}(m_z) - \text{sgn}(B)]/2$. For $|m_z| \ll 4|B|$, the low-energy continuous Hamiltonian (1) can capture the physics of the Chern insulating phases.

Symmetry-breaking perturbations. Under low-energy continuous approximation the Hamiltonian $\mathcal{H}(\mathbf{k})$ anticommutes with the symmetry operator $S = \sigma_{\vec{n}_1} \mathcal{M}_{\vec{n}_2}$. The local perturbation which breaks this symmetry includes the in-plane Zeeman fields $V_{\text{pert}} = m_x \sigma_x + m_y \sigma_y$, the nonmagnetic and magnetic disorders $\sum_{\vec{r}_j, s} V_{\text{dis}}^{\text{non}}(\vec{r}_j) n_{\vec{r}_j, s} + \sum_{\vec{r}_j, \alpha} V_{\text{dis}, \alpha}^{\text{mag}}(\vec{r}_j) \psi_{\vec{r}_j}^\dagger \sigma_\alpha \psi_{\vec{r}_j}$, with the particle number operator $n_{\vec{r}_j, s} = c_{\vec{r}_j, s}^\dagger c_{\vec{r}_j, s}$, $s = \uparrow, \downarrow$, and $\alpha = x, y, z$. Here $V_{\text{dis}}^{\text{non}}(\vec{r}_j)$ and $V_{\text{dis}, \alpha}^{\text{mag}}(\vec{r}_j)$ represent non-magnetic and magnetic random disorder potentials, respectively. In the Supplementary Information we show that the edge spin texture is not affected by the in-plane Zeeman fields without driving phase transition in the bulk, and also insensitive to the local disorder perturbations.

In the high-energy regime, due to discrete lattice anisotropy generically the Hamiltonian $\mathcal{H}(\mathbf{k})$ only anticommutes with $S = \mathcal{M}_y \sigma_x$ and $S = \mathcal{M}_x \sigma_y$. This ensures that the edge spin aligns along x (y) axis in the edges normal to \hat{e}_y (\hat{e}_x) direction and far away from sample corners. On the other hand, around the corners of the square sample the spin polarization of the high-energy edge modes can be verified to have a sizable tilt to the perpendicular direction.

Quantum tunneling transport. The tunneling transport is studied with Landauer formalism in the 2D tight-binding model of the Chern insulator. With the coupling to normal and ferromagnetic leads, we determine the retarded Green's function of the Chern insulator by $G^R(\omega) = (\omega - H - \Sigma^R)^{-1}$, where H is the tight binding Hamiltonian of the Chern insulator, and Σ^R is the self-energy due to the couplings to the leads. Using the Fisher-Lee relation we can obtain the scattering matrix based on the Green's function and self-energies [28]

$$S_{p,q}^{ss'} = -\delta_{p,q} \delta_{\alpha\beta} + i[\Gamma_p^s]^{1/2} G_{ss'}^R [\Gamma_q^{s'}]^{1/2}. \quad (4)$$

Here, the matrix element $S_{p,q}^{ss'}$ ($s, s' = \uparrow, \downarrow$) denotes the scattering amplitude of the process that an electron is scattered from the spin state s' in lead q to the spin state s in lead p , with $p \neq q = L, R$ representing the left and right-hand lead, respectively. $\Gamma_p^s = i[(\Sigma_p^{ss})^R - (\Sigma_p^{ss})^A]$, where $(\Sigma_p^{ss})^{R/A}$ is the s -spin component retarded/advanced self-energy due to the coupling to lead p . By determining the scattering matrix one can obtain the transmission coefficients regarding different spin

channels. Then we obtain the tunneling conductances under different configurations of the ferromagnetic and

normal-metal leads, and the output spin-polarized current in the spin-filtering process.

-
- [1] Haldane, F. D. M. Model for a Quantum Hall Effect without Landau Levels: Condensed-Matter Realization of the “Parity Anomaly”. *Phys. Rev. Lett.* **61**, 2015 (1988).
- [2] Klitzing, K. V., Dorda, G., & Pepper, M. New Method for High-Accuracy Determination of the Fine-Structure Constant Based on Quantized Hall Resistance. *Phys. Rev. Lett.* **45**, 494 (1980).
- [3] Tsui, D. C., Stormer, H. L. & Gossard, A. C. Two-Dimensional Magnetotransport in the Extreme Quantum Limit. *Phys. Rev. Lett.* **48**, 1559 (1982).
- [4] Chang, C. -Z. *et al.* Experimental Observation of the Quantum Anomalous Hall Effect in a Magnetic Topological Insulator. *Science*, **340**, 167 (2013).
- [5] Thouless, D. J., Kohmoto, M., Nightingale, M. P. & den Nijs, M. Quantized Hall Conductance in a Two-Dimensional Periodic Potential. *Phys. Rev. Lett.* **49**, 405 (1982).
- [6] Hasan, M. Z. & Kane, C. L. Colloquium: Topological insulators. *Rev. Mod. Phys.* **82**, 3045 (2010).
- [7] Qi, X. -L. & Zhang, S. -C. Topological insulators and superconductors. *Rev. Mod. Phys.* **83**, 1057 (2011).
- [8] Qi, X. -L., Wu, Y. -S., & Zhang, S. -C. Topological quantization of the spin Hall effect in two-dimensional paramagnetic semiconductors. *Phys. Rev. B* **74**, 085308 (2006).
- [9] Liu, C. -X., Qi, X. -L., Dai, X., Fang, Z., & Zhang, S. -C. Quantum Anomalous Hall Effect in $\text{Hg}_{1-y}\text{Mn}_y\text{Te}$ Quantum Wells. *Phys. Rev. Lett.* **101**, 146802 (2008).
- [10] Wu, C. J. Orbital analogue of the quantum anomalous Hall effect in p-band systems. *Phys. Rev. Lett.* **101**, 186807 (2008).
- [11] Yu, R. *et al.* Quantized Anomalous Hall Effect in Magnetic Topological Insulators. *Science*, **329**, 61 (2010).
- [12] Liu, X. -J., Liu, X., Wu, C., & Sinova, J. Quantum anomalous Hall effect with cold atoms trapped in a square lattice. *Phys. Rev. A* **81**, 033622 (2010).
- [13] Nomura, K. & Nagaosa, N. Surface-Quantized Anomalous Hall Current and the Magnetoelectric Effect in Magnetically Disordered Topological Insulators. *Phys. Rev. Lett.* **106**, 166802 (2011).
- [14] Zhang, H. *et al.* Topological insulators in Bi_2Se_3 , Bi_2Te_3 and Sb_2Te_3 with a single Dirac cone on the surface. *Nature Phys.* **5**, 438 (2009).
- [15] Xia, Y. *et al.* A tunable topological insulator in the spin helical Dirac transport regime. Observation of a large-gap topological-insulator class with a single Dirac cone on the surface. *Nature Phys.* **5**, 398 (2009).
- [16] Qi, X.-L., Hughes, T. L., & Zhang, S.-C. Topological field theory of time-reversal invariant insulators. *Phys. Rev. B* **78**, 195424 (2008).
- [17] Liu, X.-J., Law, K. T. & Ng, T. K. Realization of 2D Spin-orbit Interaction and Exotic Topological Orders in Cold Atoms. Preprint at arXiv:1304.0291 (2013).
- [18] Lin, Y. -J., Jiménez-García, K. & Spielman, I. B. Spin-orbit-coupled Bose-Einstein condensates. *Nature* **471**, 83 (2011).
- [19] Wang, P. *et al.* Spin-Orbit Coupled Degenerate Fermi Gases. *Phys. Rev. Lett.* **109**, 095301 (2012).
- [20] Cheuk, L. *et al.* Spin-Injection Spectroscopy of a Spin-Orbit Coupled Fermi Gas. *Phys. Rev. Lett.* **109**, 095302 (2012).
- [21] Liu, X. -J., Liu, Z. -X. & Cheng, M. Manipulating Topological Edge Spins in a One-Dimensional Optical Lattice. *Phys. Rev. Lett.* **110**, 076401 (2013).
- [22] Schnyder, A. P., Ryu, S., Furusaki, A. & Ludwig, A. W. W. Topological insulators and superconductors: ten-fold way and dimensional hierarchy, *Phys. Rev. B* **78**, 195125 (2008).
- [23] Halperin, B. I. Quantized Hall conductance, current-carrying edge states, and the existence of extended states in a two-dimensional disordered potential. *Phys. Rev. B* **25**, 2185 (1982).
- [24] Wen, X. -G. Chiral Luttinger liquid and the edge excitations in the fractional quantum Hall states. *Phys. Rev. B* **41**, 12838 (1990).
- [25] Wilczek, F. Magnetic Flux, Angular Momentum, and Statistics. *Phys. Rev. Lett.* **48**, 1144 (1982).
- [26] Žutić, I., Fabian, J. & Das Sarma, S. Spintronics: Fundamentals and applications. *Rev. Mod. Phys.* **76**, 323 (2004).
- [27] Julliere, M. Tunneling Between Ferromagnetic Films, *Phys. Lett.* **54**, 225 (1975).
- [28] Fisher, D. S. & Lee, P. A. Relation between conductivity and transmission matrix. *Phys. Rev. B* **23**, 6851 (1981).

Acknowledgement

We appreciate the helpful discussions with K. T. Law, Yayu Wang, J. Sinova, Z. -X. Liu, M. Cheng, T. K. Ng, and Y. Zhou. The authors thank the support of HKRGC through Grant 605512 and through Grant HKUST3/CRF09.

Author Contributions

All authors contributed to the studies of this work, and contributed to the writing of the manuscript. X.J.L. has planned this project.

Additional Information

The authors declare no competing financial interests. Supplementary Information accompanies this paper. Materials and correspondence can be addressed to X.J.Liu.

Supplementary Information

S-1. TWO-BAND MODEL FOR QUANTUM ANOMALOUS HALL INSULATOR

The minimal realization for the quantum anomalous Hall effect is to consider a two-band model with spin-orbit coupling and magnetization. The main results in this work are not lattice configuration dependent. Here, for convenience we consider the square lattice model with the Hamiltonian given by

$$H = \sum_{\mathbf{k}} \psi_{\mathbf{k}}^{\dagger} \mathcal{H}(\mathbf{k}) \psi_{\mathbf{k}}, \quad (\text{S1})$$

where the spin basis is defined by $\psi_{\mathbf{k}} = (c_{\mathbf{k}\uparrow}, c_{\mathbf{k}\downarrow})^T$ with $c_{\mathbf{k},s}$ the electron annihilation operator in spin state $s = \uparrow, \downarrow$, and the Bloch Hamiltonian $\mathcal{H}(\mathbf{k})$ takes the form

$$\mathcal{H}(\mathbf{k}) = 2A_1 \sin k_y \sigma_x - 2A_2 \sin k_x \sigma_y + [m_z + 2B(2 - \cos k_x - \cos k_y)] \sigma_z. \quad (\text{S2})$$

In the above form we have taken the lattice constant to be $a = 1$. In the case $|m_z| \ll 4|B|$, the physics of the system can be fully governed by the low-energy Hamiltonian

$$\mathcal{H}(\mathbf{k}) = 2A_1 k_y \sigma_x - 2A_2 k_x \sigma_y + [m_z + 2B(k_x^2 + k_y^2)] \sigma_z. \quad (\text{S3})$$

The Bloch Hamiltonian can be rewritten in the form $\mathcal{H}(\mathbf{k}) = \vec{d}(\mathbf{k}) \cdot \vec{\sigma}$, where the \vec{d} -vector is defined through $d_x = 2A_1 k_y$, $d_y = -2A_2 k_x$, and $d_z = m_z + 2B(k_x^2 + k_y^2)$. The topology of the system is determined by the first Chern number, which can be calculated by

$$C_1 = \frac{1}{4\pi} \int d^2 \mathbf{k} \mathbf{n} \cdot \frac{\partial \mathbf{n}}{\partial k_x} \times \frac{\partial \mathbf{n}}{\partial k_y}, \quad \mathbf{n} = \frac{1}{|\vec{d}(\mathbf{k})|} (d_x, d_y, d_z). \quad (\text{S4})$$

The integrand in the right hand side of the above equation describes a mapping between the momentum \mathbf{k} -space to the spherical surface S^2 formed by the unit vector $\mathbf{n}(\mathbf{k})$. Therefore the first Chern invariant is given by the number of times that this mapping can cover the whole spherical surface. For each fixed momentum $k = (k_x^2 + k_y^2)^{1/2}$, the \mathbf{n} -vector can cover one circle in the $x - y$ plane. Moreover, it is easy to see that for both $k = 0$ and $k = \infty$, the unit vector $\mathbf{n}(\mathbf{k})$ points along the z or $-z$ axis. Therefore the mapping must cover integer times of the whole spherical surface. In particular, when $m_z B > 0$, the z -component of the \mathbf{n} -vector is always positive (for $m_z > 0$) or negative (for $m_z < 0$), and the number of coverage is zero. This gives that $C_1 = 0$. On the other hand, for $m_z B < 0$ and $m_z > 0$, the unit vector \mathbf{n} points to $+z$ and $-z$ directions when $k = 0$ and $k = \infty$, respectively. We then get a single coverage of the spherical surface in the mapping, and obtain the Chern number $C_1 = 1$. Finally, from the Eq. (S4) we can see that the Chern number is odd with respect to each component of $\mathbf{n}(\mathbf{k})$, and it changes sign if reversing the sign of any component n_j . With these results in mind we conclude that

$$C_1 = \text{sgn}(A_1 A_2) [\text{sgn}(m_z) - \text{sgn}(B)] / 2. \quad (\text{S5})$$

The Hall conductance of the quantum anomalous Hall insulator is given by $\sigma_{xy} = C_1 e^2 / h$, where e and h are the electron charge and Plank constant, respectively.

S-2. TOPOLOGICAL EDGE SPIN TEXTURE

We consider the isotropic low-energy Dirac Hamiltonian (S3) with $A_1 = \eta A_2$, where $\eta = \pm 1$. In this case the low-energy Hamiltonian is rotationally invariant and can be written down in the following generic form

$$\mathcal{H}(\mathbf{k}) = 2A_1 k_{n_2} \sigma_{n_1} - 2A_2 k_{n_1} \sigma_{n_2} + (m_z + 2Bk^2) \sigma_z, \quad (\text{S6})$$

where the *arbitrary* in-plane orthogonal unit vectors are $\vec{n}_1 = u\mathbf{n}_x + v\mathbf{n}_y$ and $\vec{n}_2 = -v\mathbf{n}_x + u\mathbf{n}_y$, where the coefficients satisfy $u^2 + v^2 = 1$. The components of the momenta and Pauli matrices are given by $\sigma_{n_1} = \vec{n}_1 \cdot \vec{\sigma}$, $\sigma_{n_2} = \vec{n}_2 \cdot \vec{\sigma}$, $k_{n_1} = uk_x + vk_y$, and $k_{n_2} = -vk_x + uk_y$. It can be verified that the Hamiltonian (S6) respects the chiral-like symmetry defined by $S = \sigma_{n_2} \mathcal{M}_{n_1}$ (also valid for $\sigma_{n_1} \mathcal{M}_{n_2}$), with \mathcal{M}_{n_1} representing the spatial reflection with respect to the \vec{n}_1 direction. It follows that

$$S \mathcal{H}(\mathbf{k}) S^{\dagger} = -\mathcal{H}(\mathbf{k}). \quad (\text{S7})$$

We show below that due to this symmetry the edge states of the quantum anomalous Hall insulator are in-plane spin-polarized, and exhibit topological spin texture in the boundary. In particular, we consider three different situations as illustrated in Fig. S1: the open boundary (a), the circular close boundary (b), and the generic closed boundary (c). Furthermore, we should emphasize that while we use here the Hamiltonian (S6) as an example for the study, which is relevant for the realistic experiment. the edge spin polarizations shown below are generic results for quantum anomalous Hall insulators satisfying the chiral-like symmetry given in Eq. (S7).

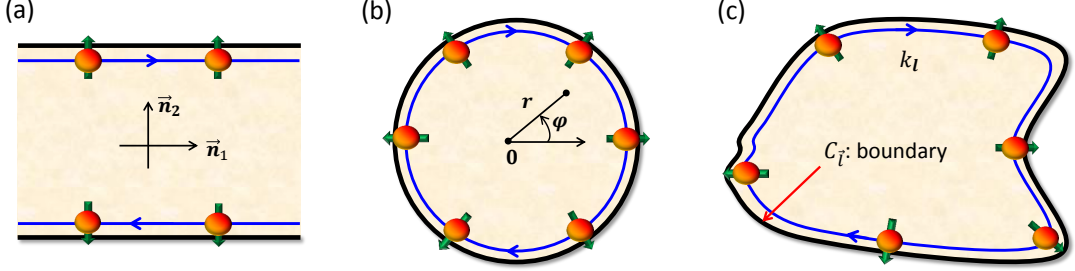


FIG. S1: Edge spin polarizations for the quantum anomalous Hall insulator with different boundary geometries. (a) The open boundary which has two edges normal to \vec{n}_2 direction, and is infinite (or periodic) along \vec{n}_1 axis; (b) The circular closed boundary which is rotationally invariant; (c) The generic boundary. In the illustration we consider the parameter regime that $m_z > 0$, $B < 0$, and $A_{1,2} > 0$.

A. Open boundary

We first consider the simplest situation that the system has two edges normal to \vec{n}_2 direction, while it is infinite (or periodic) along \vec{n}_1 axis [Fig. S1 (a)]. This study can be applied to the system with smooth and slowly varying (closed) boundaries. In this case the momenta k_{n_1} are good quantum numbers, and the Hamiltonian can be described by

$$H = \sum_{k_{n_1}} H_{1D}(k_{n_1}), \quad (\text{S8})$$

where $H_{1D}(k_{n_1})$ is a k_{n_1} -parameterized 1D Hamiltonian. The end states of $H_{1D}(k_{n_1})$ are edge states of the original 2D quantum anomalous Hall system with momentum k_{n_1} . The 1D Hamiltonian can be expressed as

$$H_{1D}(k_{n_1}) = - \int dx_{n_2} \left\{ \psi_{k_{n_1}}^\dagger(x_{n_2}) (2B\partial_{x_{n_2}}^2 \sigma_z + iA_1\partial_{x_{n_2}}\sigma_{n_1}) \psi_{k_{n_1}}(x_{n_2}) \right\} + \int dx_{n_2} \left\{ \psi_{k_{n_1}}^\dagger(x_{n_2}) [(m_z + 2Bk_{n_1}^2)\sigma_z - A_2k_{n_1}\sigma_{n_2}] \psi_{k_{n_1}}(x_{n_2}) \right\}. \quad (\text{S9})$$

The transformation in Eq. (S7) is defined for the first quantization Hamiltonian. Accordingly, for the second quantization Hamiltonian, the symmetry operator S transforms the basis according to $S(c_{k_{n_1}\uparrow}, c_{k_{n_1}\downarrow}^\dagger)^T = (c_{-k_{n_1}\downarrow}^\dagger, c_{-k_{n_1}\uparrow})^T$. This is followed by

$$SH_{1D}(k_{n_1})S^\dagger = H_{1D}(-k_{n_1}), \quad (\text{S10})$$

which gives that $SHS^\dagger = H$. It is trivial to know that at $k_{n_1} = 0$, which is a reflection invariant momentum, the 1D Hamiltonian $H_{1D}(0)$ is invariant under the S -transformation. This implies that the system $H_{1D}(0)$ belongs to the 1D chiral unitary (AIII) class [21, 22]. Indeed, this can be more transparent if rotating the spin operators $(\sigma_{n_1}, \sigma_{n_2}) \rightarrow (\sigma_y, -\sigma_x)$ in $H_{1D}(0)$. In this case, one can verify that the time-reversal and charge conjugation symmetries, defined respectively by $\mathcal{T} = iK\sigma_y$ with K the complex conjugation, and $\mathcal{C} : (\hat{c}_{k_{n_1}\sigma}, \hat{c}_{k_{n_1}\sigma}^\dagger) \rightarrow (\sigma_z)_{\sigma\sigma'} (\hat{c}_{-k_{n_1}\sigma'}^\dagger, \hat{c}_{-k_{n_1}\sigma'})$, are generically broken for H_{1D} , while at $k_{n_1} = 0$ the chiral symmetry $S = \mathcal{TC}$ is preserved. Therefore $H_{1D}(0)$ describes 1D topological insulating phase belonging to the chiral unitary (AIII) class, whose end states are eigenstates of the chiral operator σ_{n_2} , with the spin oppositely polarized in the opposite edges [21].

The spin-polarization of the edge states with $k_{n_1} \neq 0$ can be obtained using the $\mathbf{k} \cdot \mathbf{p}$ theory. By expanding up to the leading order of the momentum k_{n_1} the effective edge Hamiltonian for the two edges normal to \vec{n}_2 direction,

under the restriction of the S symmetry, should take the generic form $v_{\text{edge}}k_{\bar{n}_1}\sigma_{\bar{n}_2}$. Therefore the edge states with nonzero $k_{\bar{n}_1}$ are also eigenstates of $\sigma_{\bar{n}_2}$. The edge spin polarizations are illustrated in Fig. S1 (a) under the condition with $m_z > 0, B < 0$, and $A_{1,2} > 0$. We note that the Eqs. (S8) and (S10) are directly derived from the symmetry given in Eq. (S7), not dependent on the specific Hamiltonian (S6) or (S9). Therefore the edge spin polarizations are generic results for any 2D Hamiltonian satisfying the S symmetry.

B. Circular closed boundary

We turn to the edge spin texture for the finite system with closed boundary. For convenience we study the quantum anomalous Hall sample with circular geometry, and show below that the edge modes exhibit topological spin texture as illustrated in Fig. S1 (b). Noting that the boundary is rotationally invariant, it is convenient to reexpress the Hamiltonian in the polar coordinate (r, φ) system

$$\mathcal{H}(r, \varphi) = \left[2B \left(\frac{1}{r} \partial_r r \partial_r + \frac{1}{r^2} \partial_\varphi^2 \right) + m_z \right] \sigma_z + i \frac{2A_1}{r} \sigma_r \partial_\varphi - i 2A_2 \sigma_\varphi \partial_r, \quad (\text{S11})$$

where $\sigma_r = \cos \varphi \sigma_x + \sin \varphi \sigma_y$ and $\sigma_\varphi = \cos \varphi \sigma_y - \sin \varphi \sigma_x$. The eigenstates of $\mathcal{H}(r, \varphi)$ can generically be described by

$$|\Phi_m(r, \varphi)\rangle = |\phi_m(r, \varphi)\rangle e^{im\varphi}, \quad (\text{S12})$$

where m are integers. For bulk states, each m corresponds to two solutions $|\phi_m^{(\pm)}(r, \varphi)\rangle$, with eigenvalues $\pm E_m$ ($E_m > 0$) respectively. On the other hand, for edge modes each m corresponds to only a single eigenstate denoted by $|\phi_m^{\text{edge}}(r, \varphi)\rangle$. These states can be solved by

$$\left\{ \left[2B \left(\frac{1}{r} \partial_r r \partial_r - \frac{m^2 - i2m\partial_\varphi - \partial_\varphi^2}{r^2} \right) + m_z \right] \sigma_z - i 2A_2 \sigma_\varphi \partial_r - \frac{2A_1}{r} \sigma_r (m - i\partial_\varphi) \right\} |\phi_m^{(\pm)}(r, \varphi)\rangle = \pm E_m |\phi_m^{(\pm)}(r, \varphi)\rangle, \quad (\text{S13})$$

and

$$\left\{ \left[2B \left(\frac{1}{r} \partial_r r \partial_r - \frac{m^2 - i2m\partial_\varphi - \partial_\varphi^2}{r^2} \right) + m_z \right] \sigma_z - i 2A_2 \sigma_\varphi \partial_r - \frac{2A_1}{r} \sigma_r (m - i\partial_\varphi) \right\} |\phi_m^{\text{edge}}(r, \varphi)\rangle = \mathcal{E}_m |\phi_m^{\text{edge}}(r, \varphi)\rangle. \quad (\text{S14})$$

For the present circular boundary, the chiral-like symmetry is given by $S = \sigma_r \mathcal{M}_\varphi$, where \mathcal{M}_φ transforms φ to $-\varphi$. Using S to act on both sides of the eigen-equations for the bulk and edge states yields

$$\left\{ \left[2B \left(\frac{1}{r} \partial_r r \partial_r - \frac{m^2 + i2m\partial_\varphi - \partial_\varphi^2}{r^2} \right) + m_z \right] \sigma_z - i 2A_2 \sigma_\varphi \partial_r + \frac{2A_1}{r} \sigma_r (m + i\partial_\varphi) \right\} |\phi_{-m}^{(\pm)}(r, -\varphi)\rangle = \pm E_m |\phi_{-m}^{(\pm)}(r, -\varphi)\rangle, \quad (\text{S15})$$

and

$$\left\{ \left[2B \left(\frac{1}{r} \partial_r r \partial_r - \frac{m^2 + i2m\partial_\varphi - \partial_\varphi^2}{r^2} \right) + m_z \right] \sigma_z - i 2A_2 \sigma_\varphi \partial_r + \frac{2A_1}{r} \sigma_r (m + i\partial_\varphi) \right\} |\phi_{-m}^{\text{edge}}(r, -\varphi)\rangle = -\mathcal{E}_m |\phi_{-m}^{\text{edge}}(r, -\varphi)\rangle. \quad (\text{S16})$$

Taking that $\varphi \rightarrow -\varphi$, we can rewrite the above equations in the form

$$\left\{ \left[2B \left(\frac{1}{r} \partial_r r \partial_r - \frac{m^2 - i2m\partial_\varphi - \partial_\varphi^2}{r^2} \right) + m_z \right] \sigma_z - i 2A_2 \sigma_\varphi \partial_r + \frac{2A_1}{r} \sigma_r (m - i\partial_\varphi) \right\} |\phi_{-m}^{(\pm)}(r, \varphi)\rangle = \pm E_m |\phi_{-m}^{(\pm)}(r, \varphi)\rangle \quad (\text{S17})$$

and

$$\left\{ \left[2B \left(\frac{1}{r} \partial_r r \partial_r - \frac{m^2 - i2m\partial_\varphi - \partial_\varphi^2}{r^2} \right) + m_z \right] \sigma_z - i 2A_2 \sigma_\varphi \partial_r + \frac{2A_1}{r} \sigma_r (m - i\partial_\varphi) \right\} |\phi_{-m}^{\text{edge}}(r, \varphi)\rangle = -\mathcal{E}_m |\phi_{-m}^{\text{edge}}(r, \varphi)\rangle \quad (\text{S18})$$

From the last four formulas we find that the bulk states $|\phi_m^{(+)}(r, \varphi)\rangle$ and $|\phi_{-m}^{(-)}(r, -\varphi)\rangle$ have opposite energies E_m and $-E_m$, respectively. For edge states we have opposite energies \mathcal{E}_m and $-\mathcal{E}_m$ for $|\phi_m^{\text{edge}}(r, \varphi)\rangle$ and $|\phi_{-m}^{\text{edge}}(r, -\varphi)\rangle$, respectively. On the other hand, generically we have $E_m \neq E_{-m}$ and $\mathcal{E}_m \neq -\mathcal{E}_{-m}$ (in Eqs. (S17) and (S18)) the

left-hand side is not the original Hamiltonian). This implies that for the present circular boundary, in the edge state spectrum $\mathcal{E}_0 \neq 0$. From Eqs. (S15) and (S16) we have that the corresponding eigenstates transform according to

$$S|\phi_m^{(\pm)}(r, \varphi)\rangle = |\phi_{-m}^{(\mp)}(r, -\varphi)\rangle, \quad S|\phi_m^{\text{edge}}(r, \varphi)\rangle = |\phi_{-m}^{\text{edge}}(r, -\varphi)\rangle. \quad (\text{S19})$$

Furthermore, we note that the reflection operator \mathcal{M}_φ transforms the bulk and edge states via

$$\mathcal{M}_\varphi|\phi_m^{(\pm)}(r, \varphi)\rangle = |\phi_{-m}^{(\pm)}(r, -\varphi)\rangle, \quad \mathcal{M}_\varphi|\phi_m^{\text{edge}}(r, \varphi)\rangle = |\phi_{-m}^{\text{edge}}(r, -\varphi)\rangle. \quad (\text{S20})$$

Together with the results in Eqs. (S19) and (S20) we can deduce for the bulk and edge states that (up to \pm signs)

$$\sigma_r|\phi_m^{(\pm)}(r, \varphi)\rangle = |\phi_m^{(\mp)}(r, \varphi)\rangle, \quad \sigma_r|\phi_m^{\text{edge}}(r, \varphi)\rangle = |\phi_m^{\text{edge}}(r, \varphi)\rangle. \quad (\text{S21})$$

This shows that the edge modes are eigenstates of σ_r and then the edge spin polarization takes the spatial configuration illustrated in Fig. S1 (b) (with the parameter regime that $m_z > 0, B < 0$, and $A_{1,2} > 0$), while the bulk states are generically not eigenstates of σ_r and do not exhibit topological spin texture in the position space.

C. Generic boundary

Now we generalize the above results to the situation with generic boundary geometries [Fig. S1 (c)]. We require that in the sample there are no narrow areas where the edge modes localized in different edges may couple to each other, leading to the finite size effects. Let the boundary be characterized by a curve $C_{\vec{l}}: f(r, l) = 0$, with (r, l) consisting of a local orthogonal coordinate system. Around the boundary, one can always locally describe the Hamiltonian by

$$\mathcal{H}(r, l) = [2B(p_r^2 + p_l^2) + m_z]\sigma_z + 2A_1 p_l \sigma_r - 2A_2 p_r \sigma_l, \quad (\text{S22})$$

where p_l and p_r are momentum operators with respect to the local tangent (\vec{n}_l) and normal (\vec{n}_r) directions of the boundary, respectively. The Pauli matrices $\sigma_r = \vec{n}_r \cdot \vec{\sigma}$ and $\sigma_l = \vec{n}_l \cdot \vec{\sigma}$. For the above Hamiltonian the symmetry operator is defined by $S = \sigma_r \mathcal{M}_l$. Similarly, the edge states can be described by $|\Phi_{k_l}^{\text{edge}}(r, l)\rangle$, with k_l the quasi-momentum along the boundary. Through the same procedure as done in the above subsection, we can verify that the eigenvalues for $|\Phi_{k_l}^{\text{edge}}(r, l)\rangle$ and $|\Phi_{-k_l}^{\text{edge}}(r, -l)\rangle$ are \mathcal{E}_{k_l} and $-\mathcal{E}_{k_l}$, respectively. The transformations on these states satisfy $S|\Phi_{k_l}^{\text{edge}}(r, l)\rangle = |\Phi_{-k_l}^{\text{edge}}(r, -l)\rangle$ and $\mathcal{M}_l|\Phi_{k_l}^{\text{edge}}(r, l)\rangle = |\Phi_{-k_l}^{\text{edge}}(r, -l)\rangle$. Therefore, we again have $\sigma_r|\Phi_{k_l}^{\text{edge}}(r, l)\rangle = |\Phi_{k_l}^{\text{edge}}(r, l)\rangle$ up to a \pm sign. These results conclude that the edge states exhibit topological spin texture in the boundary.

The topological edge spin texture leads to a nontrivial quantized Berry phase in the boundary, which can be calculated by

$$\gamma_C = \oint d\tilde{x} \mathcal{A}_s(\tilde{x}), \quad \mathcal{A}_s = i\hbar \langle \chi_s(\tilde{x}) | \partial_x | \chi_s(\tilde{x}) \rangle, \quad (\text{S23})$$

where we have denoted by $|\chi_s(\tilde{x})\rangle$ the spin part of the edge state wave function, with \tilde{x} the coordinate along the boundary. Due to the topological spin texture, the Berry phase reads $\gamma_C = \pm\pi$, which defines a 1D topological state characterized by the winding number $\mathcal{N}_{1d} = \gamma_C/\pi$ in the edge. Note that the Berry phase is determined by the two in-plane spin components, it should be odd under the transformation by \mathcal{M}_{n_2} or \mathcal{M}_{n_1} , and be even under the transformation $\sigma_z \rightarrow -\sigma_z$. Therefore the 1D winding number is given by $\mathcal{N}_{1d} = \text{sgn}(A_1 A_2)$, and it has a correspondence to the bulk Chern number via

$$C_1 = \text{sgn}(m_z) \mathcal{N}_{1d}. \quad (\text{S24})$$

It is worthwhile to note that there is an additional sign factor in the correspondence between the 2D bulk topological state and the 1D topological state in the boundary. This is reasonable, since the first Chern invariant is a 2D winding number, and it necessitates the inclusion of one more dimension relative to that for \mathcal{N}_{1d} . The additional sign factor accounts for such difference in the dimension.

S-3. SYMMETRY-BREAKING PERTURBATIONS

In the low-energy regime, the nonperturbed Hamiltonian is rotationally invariant and respect the chiral-like S symmetry. The local perturbation which breaks this symmetry includes the in-plane Zeeman fields, the nonmagnetic and magnetic disorders. In the high-energy regime, due to discrete lattice anisotropy the chiral-like symmetry is generically broken in the Bloch Hamiltonian, unless for several special directions.

A. In-plane magnetic fields

The in-plane Zeeman couplings $V_{\text{pert}} = m_x \sigma_x + m_y \sigma_y$ can break the S symmetry. For the sake of generality, we write down the Hamiltonian in the bases of momenta and Pauli matrices with respect to the generic orthogonal unit vectors \vec{n}_1 and \vec{n}_2

$$\mathcal{H}(\mathbf{k}) = (2A_1 k_{n_2} + m_1) \sigma_{n_1} - (2A_2 k_{n_1} + m_2) \sigma_{n_2} + (m_z + 2Bk^2) \sigma_z, \quad (\text{S25})$$

where $m_1 = um_x + vm_y$ and $m_2 = vm_x - um_y$. The in-plane Zeeman fields shift the bulk band edge from the Γ point to the one with finite momenta. In the parameter regime $m_z B < 0$, increasing the Zeeman field can lead to a topological phase transition at the critical point

$$m_{\parallel} = m_{\parallel}^c = 2^{1/2} A \frac{|m_z|^{1/2}}{|B|^{1/2}}, \quad (\text{S26})$$

where $m_{\parallel} = (m_x^2 + m_y^2)^{1/2}$ and $A = |A_{1,2}|$. The condition with $m_{\parallel} < m_{\parallel}^c$ corresponds to the topological phase. Similar as the study in the subsection II (A), we consider the boundary modes localized in the two edges normal to \vec{n}_2 direction. It is straightforward to verify that for $S = \sigma_{\sigma_{n_2}} \mathcal{M}_{n_1}$ we have

$$S \mathcal{H}(\mathbf{k}) S^\dagger = -\mathcal{H}(\mathbf{k}) - 2m_2 \sigma_{n_2}. \quad (\text{S27})$$

Therefore, in the presence of in-plane Zeeman fields, generically no symmetry is preserved for the system. However, it is interesting that the Hamiltonian also satisfies

$$\sigma_{n_2} \mathcal{H}(\mathbf{k}) \sigma_{n_2}^{-1} = -\mathcal{H}(\mathbf{k}) - 2(m_2 + 2A_2 k_{n_1}) \sigma_{n_2}. \quad (\text{S28})$$

This implies that the Hamiltonian $\mathcal{H}_{1D}(k_{n_1}^0, x_{n_2})$ with $k_{n_1}^0 = -m_2/(2A_2)$ again defines a 1D chiral unitary (AIII) class insulator [21, 22]. Then in the topological phase the edge states localized in the left-hand side $|\Phi_{k_{n_1}^0}^{\text{edge}}(x_2)\rangle_L$ and right-hand side $|\Phi_{k_{n_1}^0}^{\text{edge}}(x_2)\rangle_R$ are eigenstates of σ_{n_2} , with the spin oppositely polarized in the opposite edges [21]. Furthermore, for the generic 1D momentum $k_{n_1} = k_{n_1}^0 + \tilde{k}_{n_1}$, we shift the zero point of the momentum to $k_{n_1}^0$, and can then rewrite the Hamiltonian in the form

$$\begin{aligned} H_{1D}(\tilde{k}_{n_1}, x_{n_2}) = & - \int dx_{n_2} \left\{ \psi_{k_{n_1}}^\dagger(x_{n_2}) (2B \partial_{x_{n_2}}^2 \sigma_z + iA_1 \partial_{x_{n_2}} \sigma_{n_1}) \psi_{k_{n_1}}(x_{n_2}) \right\} \\ & + \int dx_{n_2} \left\{ \psi_{k_{n_1}}^\dagger(x_{n_2}) [(\tilde{m}_z + 2B\tilde{k}_{n_1}^2) \sigma_z - A_2 \tilde{k}_{n_1} \sigma_{n_2}] \psi_{k_{n_1}}(x_{n_2}) \right\}, \end{aligned} \quad (\text{S29})$$

where $\tilde{m}_z = m_z + 4Bk_{n_1}^0 \tilde{k}_{n_1} + 2B\tilde{k}_{n_1}^2$. It can be seen that the above 1D Hamiltonian is *formally* equivalent to the one in Eq. (S9). Therefore, according to the previous results, all the boundary states localized in the edges normal to \vec{n}_2 direction are eigenstates of σ_{n_2} . With this result we confirm that the edge spin texture cannot be affected by the in-plane Zeeman fields without driving the phase transition in the bulk.

B. Magnetic and non-magnetic disorders

The nonmagnetic and magnetic disorders can also break the chiral-like symmetry S of the system. For convenience we adopt the lattice model to study the disorder effects. The local on-site magnetic and nonmagnetic disorders can be described by

$$V_{\text{dis}} = \sum_{\vec{r}_j, s} V_{\text{dis}}^{\text{non}}(\vec{r}_j) n_{\vec{r}_j, s} + \sum_{\vec{r}_j, \alpha} V_{\text{dis}, \alpha}^{\text{mag}}(\vec{r}_j) \psi_{\vec{r}_j}^\dagger \sigma_\alpha \psi_{\vec{r}_j}, \quad (\text{S30})$$

where $\psi_{\vec{r}_j} = (c_{\vec{r}_j, \uparrow}, c_{\vec{r}_j, \downarrow})$, the particle number operator $n_{\vec{r}_j, s} = c_{\vec{r}_j, s}^\dagger c_{\vec{r}_j, s}$ with \vec{r}_j the 2D coordinate for lattice sites, $s = \uparrow, \downarrow$, and $\alpha = x, y, z$. Here $V_{\text{dis}}^{\text{non}}(\vec{r}_j) \in [-V_0/2, V_0/2]$ and $V_{\text{dis}, \alpha}^{\text{mag}}(\vec{r}_j) \in [-V_\alpha/2, V_\alpha/2]$ represent nonmagnetic and magnetic random disorder potentials, respectively, and for magnetic disorder we take that $V_x^2 + V_y^2 + V_z^2 = V_0^2$. The configuration averaging of the disorder potentials vanishes

$$\langle V_{\text{dis}}^{\text{non}}(\vec{r}_j) \rangle = \langle V_{\text{dis}, \alpha}^{\text{mag}}(\vec{r}_j) \rangle = 0. \quad (\text{S31})$$

In the regime that the disorder strength is weak relative to the bulk gap of the quantum anomalous Hall insulator, we expect that the chiral edge spin texture cannot be scattered. The reason is because the spin chirality of the edge states ensures that edge modes with opposite spin polarizations are spatially localized far away from each other, and weak disorder, while breaking the symmetry of the bulk Hamiltonian, cannot lead to the scattering between such two edge modes. If we consider only the nonmagnetic disorder, the commutation relation between $S = \sigma_{n_2} \mathcal{M}_{n_1}$ and the second quantization Hamiltonian satisfies

$$SHS^\dagger = H - \sum_{\vec{r}_j, s} V_{\text{dis}}^{\text{non}}(\vec{r}_j) n_{\vec{r}_j, s}, \quad (\text{S32})$$

where the condition $\langle V_{\text{dis}}^{\text{non}}(\vec{r}_j) \rangle = 0$ has been applied. On the other hand, if there is only magnetic disorder, we have

$$SHS^\dagger = H - \sum_{\vec{r}_j} V_{\text{dis}, n_2}^{\text{mag}}(\vec{r}_j) \psi_{\vec{r}_j}^\dagger \sigma_{n_2} \psi_{\vec{r}_j}. \quad (\text{S33})$$

Comparing with the formulas (S32) and (S33) we can see that under the same strength of disorder potentials, the topological spin texture should be more insensitive to the magnetic disorders. This is because, for example, for the edges normal to \vec{n}_2 direction, only the magnetic disorder component $V_{n_2}^{\text{mag}}$ breaks the S symmetry and may affect the edge spin polarizations. In particular, the magnetic disorder with polarization along z direction has no effect on the edge spin texture.

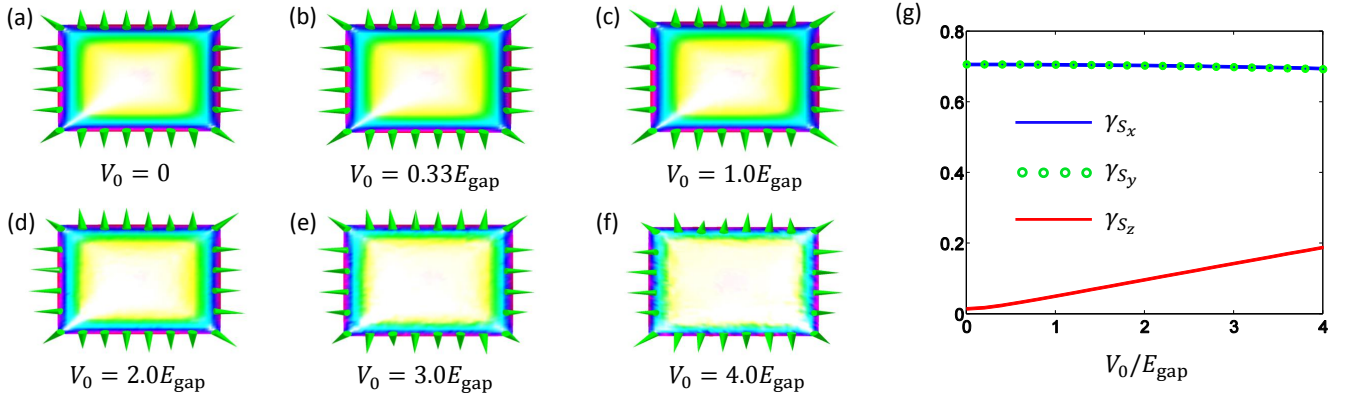


FIG. S2: Effect of nonmagnetic disorder scattering on the edge spin texture. The parameters for the numerical calculation are rescaled to be dimensionless and are taken as $A_1 = A_2 = -B = 1.0$ and $m_z = 0.3$. (a-f) The edge spin configuration with different magnitudes of the nonmagnetic disorder potential V_0 . The colors represent the wave-function distribution of the edge states; (g) Root Mean Square for S_x , S_y and S_z versus V_0 .

The numerical results for nonmagnetic and magnetic disorder effects are shown in Fig. S2 and Fig. S3, respectively. The effects of disorder scattering on the spin textures are shown in (a) to (f) in the two figures, from which one can see that the topological spin texture is nearly unaffected even when the disorder strength equals the bulk gap E_{gap} . In Fig. S2 (g) and Fig. S3 (g) we show the Root Mean Square of x , y , and z components of the edge spin

$$\gamma_{S_\alpha} = [\langle S_\alpha^2 \rangle]^{1/2}, \quad \alpha = x, y, z, \quad (\text{S34})$$

with these spin components satisfying

$$\langle S_x^2 \rangle + \langle S_y^2 \rangle + \langle S_z^2 \rangle = 1. \quad (\text{S35})$$

The magnitude of γ_{S_z} quantitatively reflects the deviation of the spatial spin configuration from the in-plane topological spin texture. It can be seen that γ_{S_z} exhibits a very weak dependence on the disorder scattering, especially in weak (magnetic and nonmagnetic) disorder regime with $V_0 < 0.2E_{\text{gap}}$ [Fig. S2 (g) and Fig. S3 (g)]. Even in the strongest disorder regime with $V_0 = 4.0E_{\text{gap}}$, the relative Root Mean Square $p = \gamma_{S_z} / (\gamma_{S_x} + \gamma_{S_y} + \gamma_{S_z})$ is less than 12% for nonmagnetic disorder and less than 9% for magnetic disorder. Under the same disorder strength, the edge spin texture is clearly more insensitive to magnetic disorder scattering, consistent with the results in Eqs. (S32) and (S33). The weak dependence of the edge spin texture on disorder scattering implies that the proposed topological spin devices in the main text are also insensitive to the local disorder perturbations.

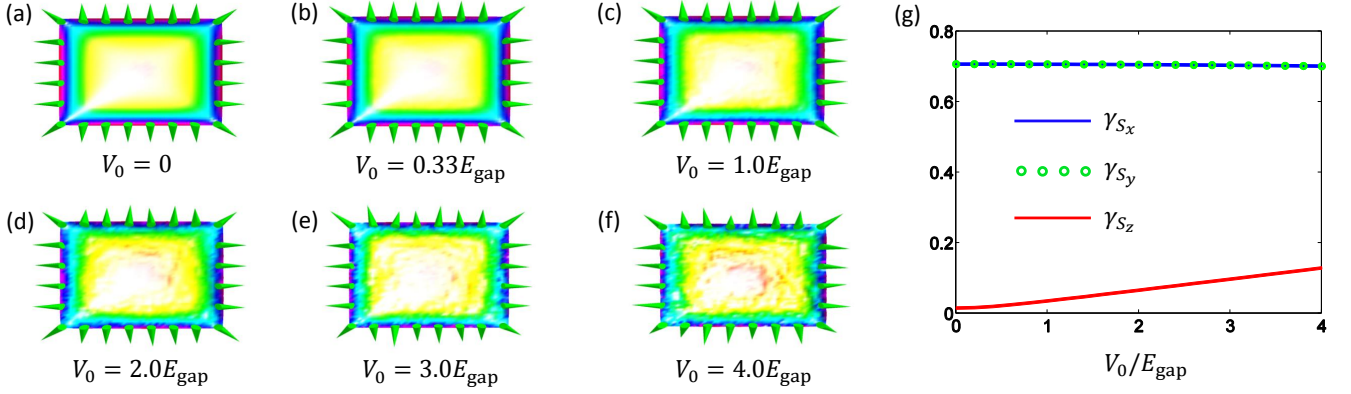


FIG. S3: Effect of magnetic disorder scattering on the edge spin texture. The parameters for the numerical calculation are the same as those in Fig. S2 $A_1 = A_2 = -B = 1.0$ and $m_z = 0.3$. (a-f) The edge spin configuration with different magnitudes of the total magnetic disorder potential $V_0 [= (V_x^2 + V_y^2 + V_z^2)^{1/2}]$; (g) Root Mean Square for $S_{x,y,z}$ versus disorder strength V_0 . Relative to the nonmagnetic disorder regime, the magnetic disorder has a stronger effect in randomizing the wave-function distribution of edge states, but clearly has a weaker scattering effect on the spin texture.

C. Effect of discrete lattice structure anisotropy

The topological spin texture relies on the continuous approximation of the Bloch Hamiltonian, which is valid in the low-energy regime. For the realistic materials [4, 11], the bulk gap of the quantum anomalous Hall insulator is much less than the bandwidth of the system. In this case, all physics, including the topology and the edge states, can be captured by the low-energy Bloch Hamiltonian. Therefore the continuous approximation is typically well justified.

The topological spin texture can in principle be scattered by the discrete lattice anisotropy in the high-energy regime. Indeed, if we consider the parameter regime that $|m_z|$ is close to or larger than $|A_{1,2}|$ and $|B|$, the bulk gap of the system is in the order of the band width. Then the high-energy edge states exist and to study them one has to go beyond the low-energy Bloch Hamiltonian. From Eq. (S2) one can see that in the high-energy regime, due to discrete lattice anisotropy generically the Bloch Hamiltonian $\mathcal{H}(\mathbf{k})$ only anticommutes with $S = \mathcal{M}_y \sigma_x$ and $S = \mathcal{M}_x \sigma_y$. This ensures that for a square sample with boundaries along the directions of Bravais lattice vectors, the edge spin aligns along x (y) axis in the edges normal to y (x) direction and far away from sample corners. On the other hand, around the corners of the square sample the spin polarization of the high-energy edge modes may have a finite tilt to the perpendicular direction due to the broken down of the S symmetry.

The numerical results are shown in Fig. S4, where we take the parameters which are rescaled to be dimensionless that $A_1 = A_2 = -B = 1.0$ and $m_z = 1.5$. In this regime the bulk band gap of the system $E_{\text{gap}} = 3.0$, which is close to the bandwidth. It can be seen from Fig. S4 (a) that the edge states with energies $|E| < 0.5$ exhibit topological spin texture, with spin polarization well within $x - y$ plane and having negligible spin tilting to z direction at the corners. However, when energy increases, the edge spins at corners exhibit a more and more pronounced tilt to the perpendicular direction. On the other hand, once going away from the corners by only few sites, we can find that the edge spins exactly point to x or y direction for all edge modes, reflecting that the chiral-like S symmetry is recovered in these directions even in the high-energy regime.

S-4. ORBITAL ANGULAR MOMENTUM FRACTIONALIZATION

The edge channel of the quantum anomalous Hall insulator can be described by 1D chiral Luttinger liquid. Furthermore, the topological spin texture leads to quantized Berry phases, which define nontrivial topological states in the boundary. Taking into account the Berry phase effect, the chiral edge states can be governed by the following effective Hamiltonian

$$H_{\text{edge}} = iv_{\text{edge}} \int d\tilde{x} \psi_s^*(\tilde{x}) [\partial_{\tilde{x}} - i\mathcal{A}_s(\tilde{x})] \psi_s(\tilde{x}). \quad (\text{S36})$$

Here ψ_s denotes the orbital wave-function of the edge states. The integral of \mathcal{A}_s along the 1D boundary gives $\oint d\tilde{x} \mathcal{A}_s(\tilde{x}) = \mathcal{N}_{1d} \pi$. The π -Berry phase is equivalent to a half magnetic flux-quanta threading through the 2D sample

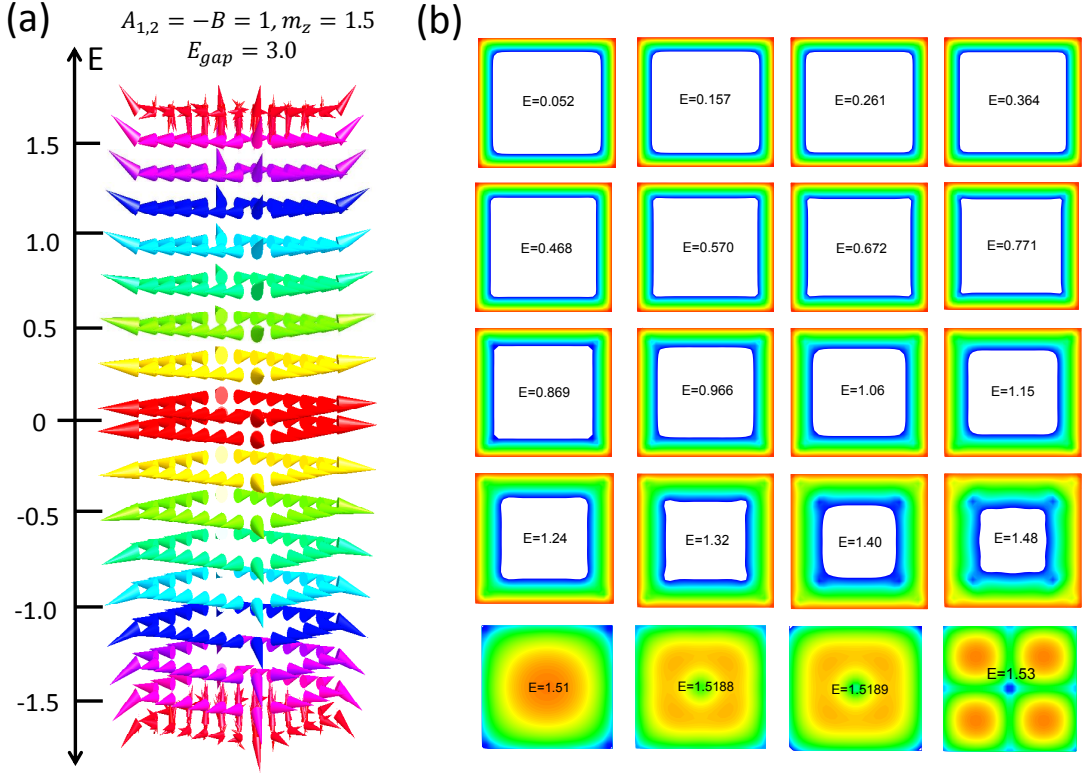


FIG. S4: Edge spin texture beyond low-energy limit in quantum anomalous Hall insulator with square boundary. The parameters are rescaled to be dimensionless that $A_1 = A_2 = -B = 1.0$ and $m_z = 1.5$, which leads to the bulk gap $E_{\text{gap}} = 3.0$. (a) The spin texture for edge modes of different energies, with only part of the states shown here. It can be seen that the edge states with energies $|E| < 0.5$ exhibit topological spin texture, with spin polarization well within $x - y$ plane. Beyond such energy scale the edge spins exhibit a more and more pronounced tilt to the perpendicular direction at square corners; (b) Wave function profiles of the edge states (for energy $E < 1.5$) and bulk states (for $E > 1.5$).

and encircled by the edge. According to the study by Wilczek in 1982 [25], a half quantum flux can lead to $1/2$ -fractionalization of the orbital angular momentum. As a result, for the 2D sample with circular geometry, the orbital angular momentum of the edge modes should be fractionalized as $l_z = m + \mathcal{N}_{1d}/2$, with m being integers. The energy spectrum of the edge states is corresponding to fractionalization of the orbital angular momentum and is given by

$$\mathcal{E}_{l_z} = (m + \frac{1}{2}\mathcal{N}_{1d}) \frac{v_{\text{edge}}}{R_{l_z}}, \quad m = 0, \pm 1, \pm 2, \dots \quad (\text{S37})$$

where R_{l_z} is the effective radius of edge state wave function. Due to the $1/2$ -fractionalization no zero-energy edge state exists. Then the number of edge states is $N = \text{even}$. This result can also be derived from the Eq. (S14). If separating the edge state wave-function by spin and orbital parts $|\phi_m^{\text{edge}}(r, \varphi)\rangle = \phi_m(r)|\chi_s(\varphi)\rangle$, from Eq. (S14) one can obtain the energy by

$$\begin{aligned} \mathcal{E}_m &= 2A_1 \langle \phi_m(r) | \frac{1}{r} | \phi_m(r) \rangle \langle \chi_s(\varphi) | \sigma_r (m - i\partial_\varphi) | \chi_s(\varphi) \rangle \\ &= (m + \frac{1}{2}) \frac{2A_1}{R_m}, \quad m = 0, \pm 1, \pm 2, \dots \end{aligned} \quad (\text{S38})$$

where R_m is the expectation value of $1/r$. Now let us thread an additional magnetic flux Φ through the sample, which is described by a gauge $\mathbf{A} = A_\varphi \hat{e}_\varphi$, with $A_\varphi = (\Phi/\Phi_0) \frac{1}{r}$, where Φ_0 represents the flux quanta. In the presence of the external magnetic flux, the equation for $|\phi_m^{\text{edge}}(r, \varphi)\rangle$ reads

$$\left\{ \left[2B \left(\frac{1}{r} \partial_r r \partial_r - \frac{(m - \Phi/\Phi_0)^2 - i2(m - \Phi/\Phi_0) \partial_\varphi - \partial_\varphi^2}{r^2} \right) + m_z \right] \sigma_z - i2A_2 \sigma_\varphi \partial_r - \frac{2A_1}{r} \sigma_r (m - \frac{\Phi}{\Phi_0} - i\partial_\varphi) \right\} |\phi_m^{\text{edge}}(r, \varphi)\rangle = \mathcal{E}_m |\phi_m^{\text{edge}}(r, \varphi)\rangle. \quad (\text{S39})$$

From the above equation one can find that the energy spectrum of edge states is shifted to be $\frac{2A_1}{R_m}(m + 1/2 - \Phi/\Phi_0)$. Therefore, when an additional magnetic 1/2-flux-quanta $\Phi = \Phi_0/2$ is threaded through the sample, the edge state $|\phi_0^{\text{edge}}(r, \varphi)\rangle$ is exactly pushed to zero energy, and the number of edge states becomes $N = \text{odd}$. The change in the number of edge modes between *even* and *odd* by threading a half flux-quanta provides an observable for the 1/2-fractionalization of orbital angular momentum.